Identification of $m = 2$ competent mode of complex magneto-hydro-dynamics activities during internal soft disruption based on singular value decomposition and tomography of soft-X-ray emission on the HT-7 tokamak*

Xu Li-Qing(徐立清), Hu Li-Qun(胡立群)†, Li Er-Zhong(李二众), Chen Kai-Yun(陈开云), Liu Zhi-Yuan(刘志远), Chen Ye-Bin(陈晔斌), Zhang Ji-Zong (张继宗), Zhou Rui-Jie(周瑞杰), Yang Mao(杨 茂), Mao Song-Tao(毛松涛), and Duan Yan-Min(段艳敏)

Institute of Plasma Physics, Chinese Academy of Sciences, Hefei 230031*, China*

(Received 27 August 2011; revised manuscript received 28 November 2011)

In this paper, the singular value decomposition (SVD) method as a filter is applied before the tomographic inversion of soft-X-ray emission. Series of 'filtered' signals including specific chronos and topos are obtained. (Here, chronos and topos are the decomposed spatial vectors and the decomposed temporal vectors, respectively). Given specific magnetic flux function with coupling $m = 1$ and $m = 2$ modes, the line-integrated soft-X-ray signals at all chords have been obtained . Then $m = 1$ and $m = 2$ modes have been identified by tomography of simulated 'filtered' signals extracted by the SVD method. Finaly, using the experimental line-integrated soft-X-ray signals, $m = 2$ competent mode of complex magnetohydrodynamics(MHD) activities during internal soft disruption is observed. This result demonstrates that $m = 2$ mode plays an important role in internal disruption (Here, m is the poloidal mode number).

Keywords: singular value decomposition, disruption, soft-X-ray tomography, tokamak

PACS: 52.70.La, 52.55.Fa, 52.65.Kj **DOI:** 10.1088/1674-1056/21/5/055208

1. Introduction

Major disruption is a serious problem for tokamak operation.[1−6] The major disruption can be due to several reasons, for example, the low-q discharge, the MHD instability and mode locking, the vertical displacement events (VDEs), and the high density operations. When the major disruption occurs, it can not only generate great heat loads on the first wall and divertor plates, but also leads to the large electromagnetic force because of the halo current. In HT-7 discharges, complex magnetohydrodynamics is always followed by major disruption or internal soft disruption.[7−11]

MHD instabilities, known as a variety of perturbation modes, play an important role in tokamak plasmas.[12] One class of the most dangerous modes is tearing-like, consisting of classic and neoclassic, which manifest themselves as island structures at low order rational surfaces.[13] The magnetic reconnection, which bridges two adjacent rational surfaces, probably leads to stochastic magnetic field transports, resulting in severe confinement deterioration.[14] That could cause disruptions in some circumstances.[15,16] Thus, understanding MHD instabilities is essential to control them.

For island structures at low order rational surfaces, especially in the case of different modes coupling, it is difficult to identify MHD mode numbers using Mirnov signals.[17] With the multiple soft-X-ray (SXR) arrays imaging system,[18−20] one can easily identify the MHD single mode number, but it is also difficult to identify MHD mode numbers in the mode coupling case by tomography of soft-X-ray emission.

SVD is a well-known mathematical tool,[21,22,25] which has been successfully used in plasma physics to investigate the spatial-temporal behavior of fluctuating quantities such as the magnetic field or SXR line-integrated data. It was used to deal with the magneto hydrodynamic data of SXR first in JET,[23] then

*Project supported by the National Natural Science Foundation of China (Grant No. 10935004).

†Corresponding author. E-mail: lqhu@ipp.ac.cn

© 2012 Chinese Physical Society and IOP Publishing Ltd

in HL-1M[24] and HT-7.[7,8,10,21] In this paper $m = 1$ and $m = 2$ coupling mode has been identified by tomography of "filtered" signals extracted by the SVD method.

The rest of this paper is organized as follows. In Section 2, application of singular value decomposition in SXR signals. In Section 3, identified $m = 1$ and $m = 2$ mode numbers using the simulated data. In Section 4, observation of $m = 2$ competent mode of complex MHD activities during internal soft disruption. Finally, the summary is given in Section 5.

2. Application of singular value decomposition in SXR signals

In the recent HT-7 experimental campaign, there are three SXR cameras on the machine. Each camera array consists of a slit and 46 channels of SXR detector, which is sensitive to photon energies from 1 to 13 keV. The thickness of the beryllium filter is about 12.5 μm. For each camera, the distance from the geometric center of the plasma to the center of the beryllium filter is 400 mm. The maximum sampling rate of this diagnostic system is 250 kHz, corresponding to the temporal resolution 4 μs. Moreover, their spatial resolution is changed from 0.6 to 1.5 cm.

One can construct the matrix from N channels SXR signals such as

$$\boldsymbol{X}_{M\times N} = \begin{bmatrix} a_{11} & a_{12} & \cdots & a_{1N} \\ a_{21} & a_{22} & \cdots & a_{2N} \\ \vdots & \vdots & \cdots & \vdots \\ a_{M-11} & a_{M-12} & \cdots & a_{M-1N} \\ a_{M1} & a_{M2} & \cdots & a_{MN} \end{bmatrix}. \quad (1)$$

The column vectors of the matrix represent the sampling data of different channels during one shot while the row vectors correspond to different sampling time-slices.[21] Equation (1) means m-fold sampling in one discharge. Then the matrix $\boldsymbol{X}_{M\times N}$ can be decomposed by SVD as follows:

$$\boldsymbol{X}_{M\times N} = \boldsymbol{U}_{M\times N} \times \boldsymbol{S}_{N\times N} \times \boldsymbol{V}_{N\times N}. \quad (2)$$

Both $\boldsymbol{U}$ and $\boldsymbol{V}$ are unitary, the columns of $\boldsymbol{U}$ represent spatial "eigenvectors" or topos whereas the columns of $\boldsymbol{V}$ can be considered as temporal "eigenvectors" or chronos.[26,27] Due to the descending order of the singular values, $\boldsymbol{X}$ is decomposed into different components of descending relative importance. The first topos/chronos pairs contain most of the information of $\boldsymbol{X}$, which is called the balanceable signal of the total SXR signal. The sum of the rest of the topos/chronos pairs is the perturbed signal of the total SXR signal. The components with the smallest singular values merely contain noise, i.e. it is possible to use SVD for filtering. If we are only interested in the n-th component we obtain a "filtered" matrix $\boldsymbol{X}_i$[17] by

$$\boldsymbol{X}_i = \boldsymbol{u}_i \times \boldsymbol{S}_i \times \boldsymbol{v}_i^{\mathrm{T}}, \quad (3)$$

where $\boldsymbol{u}_i$ and $\boldsymbol{v}_i$ stand for the n-th topos and chronos, i.e. the n-th columns of $\boldsymbol{U}$ and $\boldsymbol{V}$, respectively, and $\boldsymbol{S}_i$ is the corresponding singular value.

In order to identify the MHD mode structures, we only use the perturbed signals. We will discuss more about this in Section 3. In this paper, "filtered" matrix $\boldsymbol{X}_i$ is only under the condition that $i \geq 2$.

3. Identified $m = 1$ and $m = 2$ mode numbers using simulated data

The contour plot of the reconstructed local emission profile, by using SXR tomography, mainly reflects the pressure profile, hence the magnetic flux surface. This is the reason why using SXR tomography can obtain the magnetic flux surface. Spatial distribution of the so-called emissivity $g(r, \theta)$ can be obtained by SXR tomography, and then the magnetic flux surface is also obtained by the contour plot of $g(r, \theta)$. This is also why magnetic flux function $\psi(r, \theta)$ can be obtained by SXR tomography.

As mentioned in Section 2, balanced signals and perturbation signals can be separated by the SVD method. In order to get the mode structure of coupling MHD modes, we extracted perturbation signals from the SXR raw signals by the SVD method. Then perturbation of the local emission intensities can be obtained by using the perturbation signals for tomography. Finally, mode structures will be clearly shown by the contour plot of the reconstructed perturbation of the local emission intensities. In all, the perturbation magnetic surfaces can be obtained by using tomography of the high-resolution SXR emission together with the SVD technique.

In order to corroborate the different "filtered" signals indicated different spatial structures of MHD modes, one can use a specific magnetic flux function

$\psi(r,\theta)$, to futher obtain line-integrated SXR signals of all channels. Then using the method mentioned in Section 2, one can get a series "filtered" matrix $\boldsymbol{X}_i$. Finally using a "filtered" signal for tomographic inversion, one can separate a different single mode from a coupling mode. More details of the method will be shown with a specific sample below.

The form of the specific magnetic flux function with coupling of $m = 1$ and $m = 2$ MHD modes are given as[28]

$$\begin{aligned}\psi(r,\theta) = {} & \frac{r_0^2 + r_s^2}{2} \ln\left(\frac{r_0^2+1}{r_0^2+r^2}\right) - \frac{1-r^2}{2} \\ & - \left\{ \frac{W^2}{2} \times \frac{r_s^{2-m}}{r_0^2+r_s^2} \times \frac{r^m(1-r)}{1-r_s} \right. \\ & \times \frac{2}{1+\exp\left[10\left(1-\frac{r}{r_s}\right)\right]} \cos(m\theta+\omega t) \Big\} \\ & - \left\{ \frac{W^2}{2} \times \frac{r_s^{1-m}}{r_0^2+r_s^2} \times \frac{r^{m+1}(1-r)}{1-r_s} \right. \\ & \times \frac{2}{1+\exp\left[10\left(1-\frac{r}{r_s}\right)\right]} \\ & \left. \times \cos((m+1)\theta+2\omega t) \right\}, \end{aligned} \tag{4}$$

where W is the width of the island, r_s is the radius of the rational suface, r_0 is an effective current channel radius, ω is the frequency of the MHD mode. In this paper, $m = 1$, $W = 0.3$, $r_s = 0.3$, and $r_0 = 0.9$.

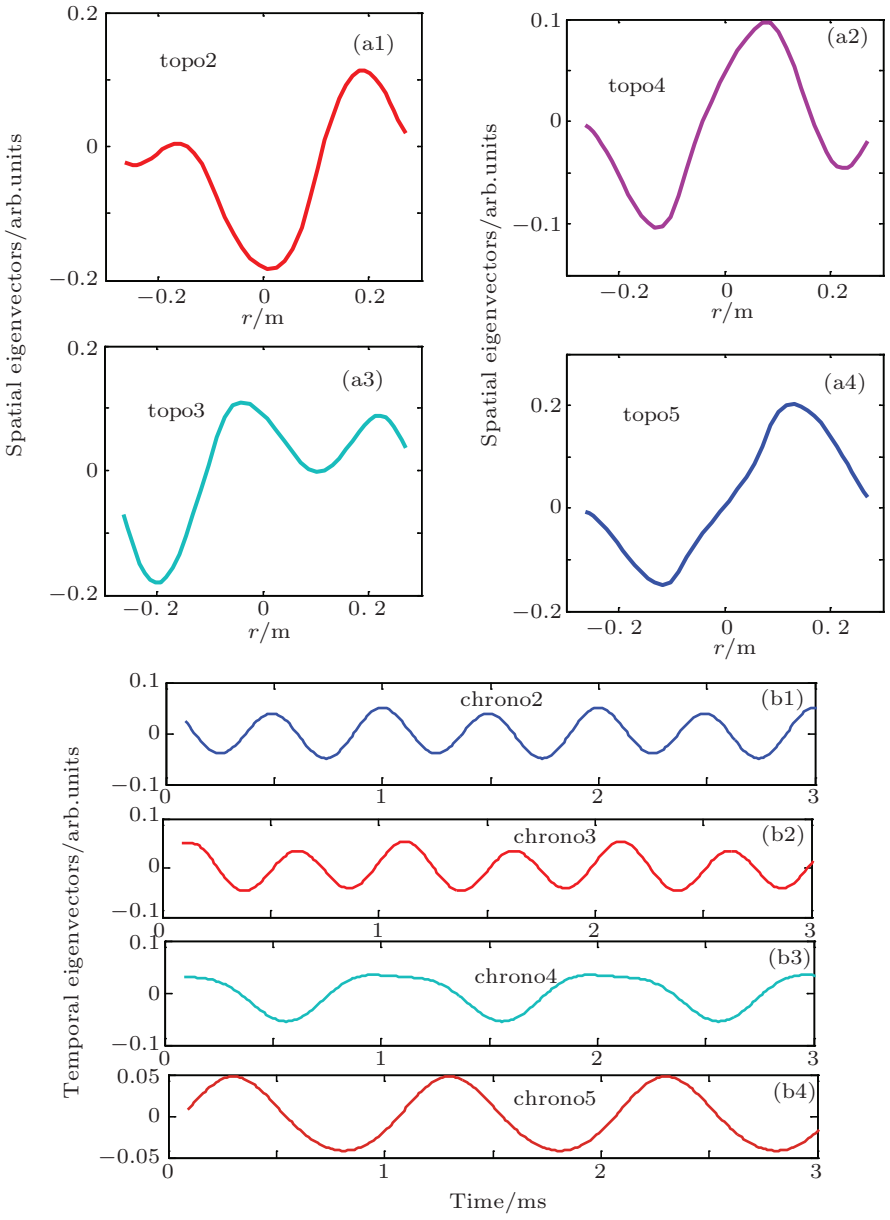


Fig. 1. (colour online) The results of SVD analysis of the simulation data. (a1)–(a4) topo2 and topo3 correspond to the spatial structure of the $m = 2$ mode. Topo4 and topo5 correspond to the spatial structure of the $m = 1$ mode. (b1)–(b4) chrono2 and chrono3 correspond to the $m = 2$ mode. Chrono4 and chrono5 give the evolution of the $m = 1$ mode.

Using Eq. (4) and the SXR imaging system of the HT-7 tokamak, one can calculate $\boldsymbol{X}_{M\times N}$. Then according to Eq. (2), the matrix $\boldsymbol{X}_{M\times N}$ can be decomposed by SVD. The results of SVD analysis are presented in Fig. 1. Focusing on topo2 to topo5, it is obvious that topo2 and topo3 (Figs. 1(a1) and 1(a3)) correspond to the spatial structure of the $m = 2$ mode and topo4 and topo5 (Figs. 1(a2) and 1(a4)) correspond to the spatial structure of the $m = 1$ mode. According to Eq. (3), one can calculate the "filtered" signal of matrix $\boldsymbol{X}_i$ ($i = 2, 3, 4, 5$). Since both topo2 and topo3 correspond to the spatial structure of the $m = 2$ mode and both topo4 and topo5 correspond to the spatial structure of the $m = 1$ mode, one can obtain the following relationship by combining $\boldsymbol{X}_2$ with $\boldsymbol{X}_3$, and $\boldsymbol{X}_4$ with $\boldsymbol{X}_5$,

$$\boldsymbol{X}_{2,3} = \boldsymbol{X}_2 + \boldsymbol{X}_3, \tag{5}$$

$$\boldsymbol{X}_{4,5} = \boldsymbol{X}_4 + \boldsymbol{X}_5. \tag{6}$$

Finally, use $\boldsymbol{X}_{2,3}$ and $\boldsymbol{X}_{4,5}$ for tomographic inversion, respectively. The results of tomography at time point $t = 2$ ms are given in Fig. 2. The results clearly show that $\boldsymbol{X}_{2,3}$ (Fig. 2(a)) corresponds to the spatial structure of the $m = 2$ mode and $\boldsymbol{X}_{4,5}$ (Fig. 2(b)) corresponds to the spatial structure of the $m = 1$ mode.

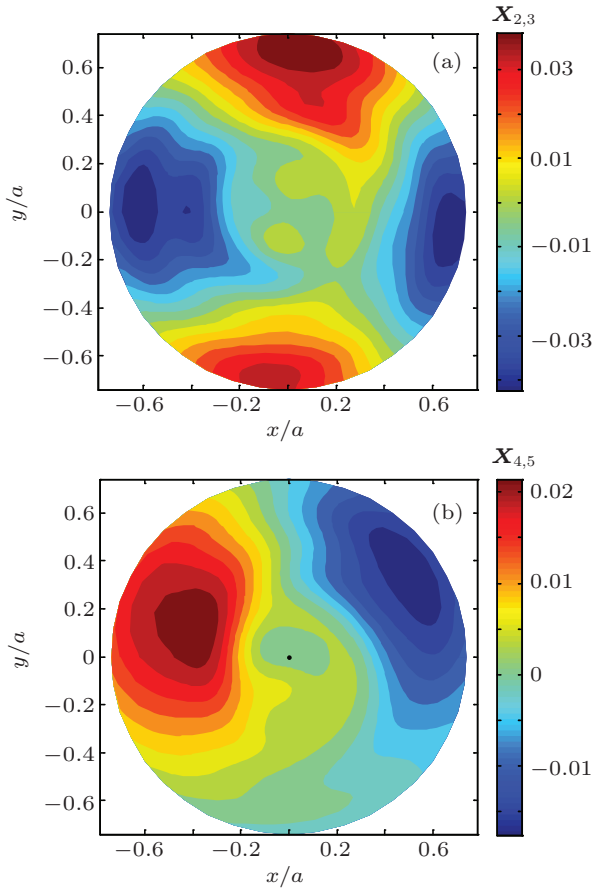


Fig. 2. (colour online) The tomographic results of perturbation of the simulated SXR signals at time point $t = 2$ ms.(a) $\boldsymbol{X}_{2,3}$ corresponds to the spatial structure of the $m = 2$ mode, (b) $\boldsymbol{X}_{4,5}$ corresponds to the spatial structure of the $m = 1$ mode. Here, $a = 27$ cm is the minor radius of the HT-7 tokamak.

4. Observation of $m = 2$ competent mode of complex MHD activities during internal soft disruption

Complex MHD activities are observed under a wide range of operating conditions in HT-7 tokamaks. Plasma discharges #111635 on the HT-7 with the following plasma parameters are analyzed: plasma current $I_\mathrm{p} \approx 150$ kA, toroidal magnetic field $B_\mathrm{t}(0) \approx 1.85$ T at the plasma center, the central chord-averaged electron density $N_\mathrm{e}(0) \approx 2.5 \times 10^{13}$ cm^{-3}. Figure 3 shows the typical complex MHD activities during internal soft disruption in shot #111635. The SXR signals are treated using the same method as described in Section 3. The results of SVD analysis are displayed in Fig. 4. Focusing on topo2 to topo5, it is clear that topo2 (Fig. 4(a1)) corresponds to the spatial structure of the $m = 1$ mode and topo8 (Fig. 4(a2)) corresponds to the spatial structure of the $m = 2$ mode. Topo3 (Fig. 4(a3)) almost corresponds to the spatial structure of the $m = 1$ mode, Topo5 (Fig. 4(a4)) by and large corresponds to the spatial structure of the $m = 2$ mode.

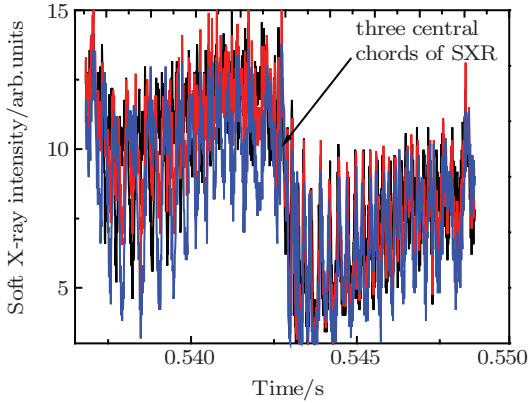


Fig. 3. (colour online) Typical complex MHD activities during internal soft disruption of the line-integrated SXR signals at three chords in shot #111635.

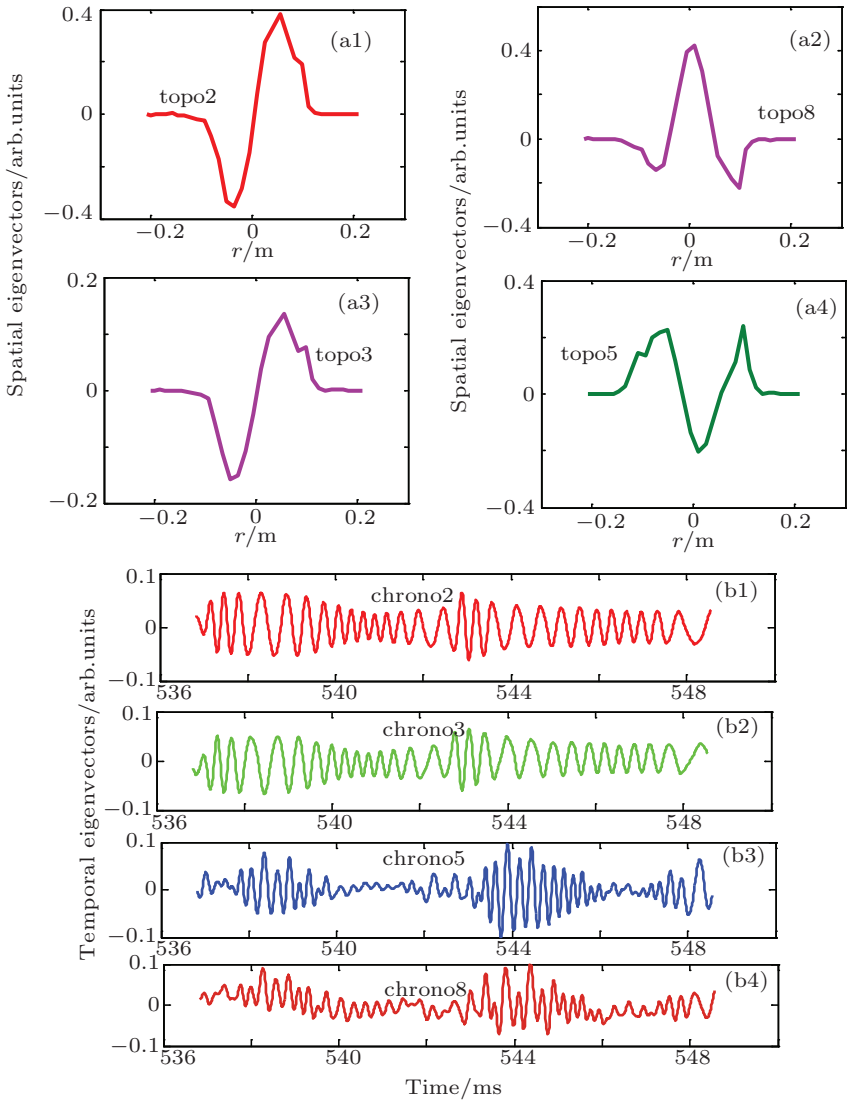


Fig. 4. (colour online) The results of SVD analysis of the MHD mode. (a1)–(a4) topo2 corresponds to the spatial structure of the $m = 1$ mode, topo8 corresponds to the spatial structure of the $m = 2$ mode. (b1)–(b4) Chrono2 corresponds to the $m = 1$ mode, chrono8 gives the evolution of the $m = 2$ mode.

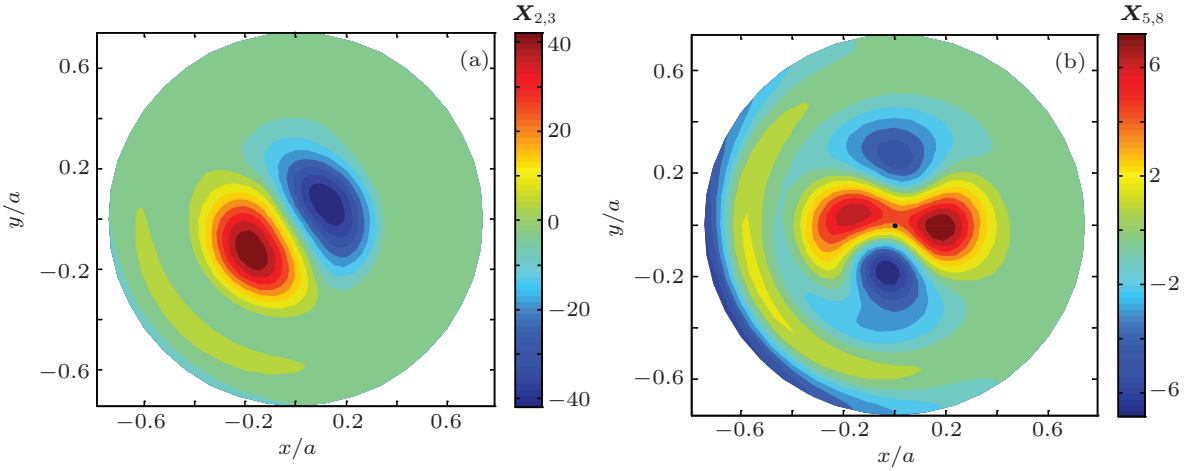


Fig. 5. (colour online) The tomographic results of MHD mode of shot #111635 at time point $t = 537.5$ ms. (a) $\boldsymbol{X}_{2,3}$ corresponds to the spatial structure of the $m = 1/n = 1$ mode, (b) $\boldsymbol{X}_{5,8}$ corresponds to the spatial structure of the $m = 2/n = 1$ mode.

Tomographic inversion are performed for $\boldsymbol{X}_{2,3}$ ($\boldsymbol{X}_2 + \boldsymbol{X}_3$) and $\boldsymbol{X}_{5,8}$ ($\boldsymbol{X}_5 + \boldsymbol{X}_8$), respectively. The results of tomography at time point $t = 537.5$ ms are shown in Fig. 5. The results clearly show $\boldsymbol{X}_{2,3}$ (Fig. 5(a)) corresponds to the spatial structure of the $m = 1$ mode and $\boldsymbol{X}_{5,8}$ (Fig. 5(b)) corresponds to the spatial structure of the $m = 2$ mode.

5. Summary

SVD as an effective instrument of filter is applied to analyze the data of SXR. The temporalvectors chronos of SVD can indicate the period of sawtooth, and the vectors topos can give spacial properties of sawtooth, e.g., the mode structure of precursor of sawtooth.

Together with SVD and tomography of the high-resolution SXR emission, MHD coupling mode structure can be separated. On HT-7 discharges, $m = 2$ competent mode of complex MHD activities during internal soft disruption has been identified. It shows that $m = 2$ mode must have played an important role in the progress of plasma disruption. However, suppressing $m = 2$ mode is beyond the scope of this paper.

References

[1] Liu Y, Yan J C, Zhou C P, Ding X T, Wang S J, Wang E Y, Yao L H , Mao W C, Pan C H, HL-1M team and HL-2A team 2004 *Nucl. Fusion* **44** 372

[2] Yang Q W, Ding X T, Yan L W, Xuan W M, Liu D Q, Chen L Y, Song X M, Yuan B S, Zhang J H, Gao Z, Li X D, Mao W C, Zhou C P, Wang E Y, Liu Y and HL-1M team 2004 *Chin. Phys. Lett.* **21** 2475

[3] Yang Q W, Ding X T, Shi Z B, Pan Y D, Cao Z, Zhou Y, Liu Y, Cui Z Y, Li W, Feng B B, Yang J W, Song X Y, Liu Z T, Deng Z C, Zheng Y Z, Liu Y and HL-2A team 2005 *32nd EPS Conference on Plasma Phys. Tarragona*

[4] Murakami M, Callen J D and Berry L A 1976 *Nucl. Fusion* **16** 347

[5] Greenwald M, Terry J L, Wolfe S M, Bell M G, Kaye S M and Neilson G H 1988 *Nucl. Fusion* **28** 2199

[6] Carreras B, Hicks H R, Holmes J A and Waddell B V 1980 *Phys. Fluids* **23** 1811

[7] Chen K Y, Hu L Q, Duan Y M, Ma T P and HT-7 team 2008 *Phys. Lett.* A **372** 4469

[8] Ma T P, Hu L Q, Wan B N, Ruan H L, Gao X, Zhen X J, Zhou L W , Sun Y W, Chen Z Y, Lin S Y and Kong W 2005 *Chin. Phys.* **14** 2061

[9] Sun Y W, Wan B N, Hu L Q ,Wang S J, Shen B, Zhang X Q, Zhen X J and Xu G S 2005 *Plasma Phys. Control. Fusion* **47** 745

[10] Sun Y W, Wan B N, Hu L Q and Shen B 2007 *Nucl. Fusion* **47** 271

[11] Sun Y W, Wan B N, Hu L Q, Chen K Y, Shen B and Mao J S 2009 *Plasma Phys. Control. Fusion* **51** 065001

[12] Hender T C, Wesley J C, Bialek J, *et al* 2007 *Nucl. Fusion* **47** S128

[13] Hegna C C 1998 *Phys. Plasmas* **5** 1767

[14] Udintsev V S, Milligen B H, Schüller F C, Krämer F A, Donné A J H, Gorkom J C, Domier C W and the TEXTOR-team 2003 *Nucl. Fusion* **43** 1424

[15] Eastwood J W and Wayne A 1986 *Phys. Rev. Lett.* **57** 2528

[16] Howling A A and Robinson D C 1988 *Plasma Phys. Control. Fusion* **30** 1863

[17] Kim J S, Edgell D H, Greene J M and Chance M S 1999 *Plasma Phys. Control. Fusion* **41** 1399

[18] Meng S J, Li Z H and Q Y 2011 *Acta Phys. Sin.* **60** 418 (in Chinese)

[19] Tsuji S, Nagayama Y, Kawahata K and Tanahashi S 1982 *Nucl. Fusion* **22** 1082

[20] Wang X F and Wang J Y 2011 *Acta Phys. Sin.* **60** 025212 (in Chinese)

[21] Li E Z, Ling B L, Liu Y ,Ti A, Hu L Q and Gao X 2010 *Chin. Phys.* B **19** 035203

[22] Anton M, Weisen H, Dutch M J , Linden, F B, Chavan R, Marletaz B, Marmillod P and Paris P 1996 *Plasma Phys. Control. Fusion* **38** 1849

[23] Nardonet C 1992 *Plasma Phys. Control. Fusion* **34** 1447

[24] Dong Y B, Pan C H, Liu Y and Fu B Z 2004 *Plasma Sci. Technol.* **6** 2307

[25] Press W H, Teukolsky S A, Vetterling W T and Flannery B P 1992 *Numerical Recipes in FORTRAN: The Art of Scientific Computing* (Cambridge: Cambridge University Press)

[26] Dudok W T, Pecquet A L, Vallet J C and Lima R 1994 *Phys. Plasmas* **1** 3288

[27] Zohm H, Greene J M, Lao L L and Strait E J 1992 *General Atomics Technical Report* GA-A20886 SanDiego

[28] Navarro A P, Paré V K and Dunlap J L 1981 *Rev. Sci. Instrum.* **52** 1634